

A tau scenario application to a search for upward-going showers with the Fluorescence Detector of the Pierre Auger Observatory

Ioana Alexandra Caracas^{a,*} on behalf of the Pierre Auger^b Collaboration
(a complete list of authors can be found at the end of the proceedings)

^a Bergische Universität Wuppertal, Department of Physics, Gaußstraße 20, Wuppertal, Germany

^b Observatorio Pierre Auger, Av. San Martín Norte 304, 5613 Malargüe, Argentina

Full author list: http://www.auger.org/archive/authors_icrc_2021.html

E-mail: spokespersons@auger.org

Recent observations of two coherent radio pulses with the ANITA detector can be interpreted as steeply upward-going cosmic-ray showers with energies of a few tenths of an EeV and remain unexplained. The Pierre Auger Observatory has a large exposure to such upward propagating shower-like events, and has used 14 years of its Fluorescence Detector (FD) data to perform a generic search for such events with elevation angles greater than 20° from the horizon. Here this search is recast to constrain models generating high energy τ -leptons. For maximal flexibility, only the propagation, decay, and interactions of τ -leptons are treated in this analysis, meaning that the results are independent of the τ -production scenario. This treatment allows for the application of these results to the wide range of models producing τ -leptons that have been proposed to describe the "anomalous" ANITA events. The goal of this study is accomplished by generating τ -leptons within the Earth and its atmosphere with an intensity dependent on the media density. The zenith angle, location and calorimetric energy of any resulting τ -induced air showers are then used to calculate the exposure of the FD of the Pierre Auger Observatory to τ primaries. Differential limits as low as $10^{-9} \text{ GeV s}^{-1} \text{ cm}^{-2} \text{ sr}^{-1}$ to the flux of τ -leptons produced with less than a 50 km path length below the Earth's surface are reported for several zenith angle ranges and primary energy spectra. Full exposure and sensitivity information is provided, facilitating the application of these results to different τ -lepton production models.

37th International Cosmic Ray Conference (ICRC 2021)
July 12th – 23rd, 2021
Online – Berlin, Germany

*Presenter

1. Introduction

The ANITA collaboration reported the observation of two up-going cosmic ray-like events that were observed in the first and third ANITA flights. The two events were reconstructed with moderately high elevation angles of $27.4^\circ \pm 0.3^\circ$ and $35.0^\circ \pm 0.3^\circ$, and their energies were initially reported to be 0.6 ± 0.4 EeV and $0.56^{+0.3}_{-0.2}$ EeV, respectively [1]. Later they were reanalyzed with dedicated simulations and the reconstructed energy was shown to depend on the altitude of the "injection point" at which the shower begins to develop in the atmosphere. From this, a minimum shower energy of 0.2 EeV was found for both events [2]. Up-going air showers of that kind can be potentially explained by particles penetrating the Earth with very low cross section. As the τ -lepton has a range that can reach 50 km in rock at ultra-high energies, the conversion of high energy τ -neutrinos into τ -leptons was considered as one possible explanation. However, this interpretation was dismissed because of the large attenuation of neutrinos in the Earth for these energies and elevation angles. The corresponding diffuse neutrino flux that would be required to explain the two events exceeds the flux constraints published by IceCube and Auger [2–4] by far. For this reason these events are often referred to as "anomalous" ANITA events. Neutrinos of these energies are actually unlikely to be observed with elevation angles greater than a few degrees below the horizon [5, 6]. The observation of these two up-going events with steep exit angles and high energies is in strong disagreement with the Standard Model of particle physics [7].

Due to the surprising nature of these events, there is a distinct need for follow-up studies to independently verify the ANITA observations. The Pierre Auger Observatory has been used to set competitive limits to neutrino fluxes with its surface detector array. The detector is particularly sensitive to τ -neutrinos interacting in the Earth, but only for very low emerging angles, typically of one or two degrees. The surface array cannot detect showers with the elevation angles of these anomalous events. However, using the telescopes that constitute the Fluorescence Detector, *FD*, of the Observatory, we can directly observe the evolution of air showers in the atmosphere by collecting the fluorescence light emitted as the air shower develops. As the light emission is proportional to the energy deposit in the atmosphere, it measures the calorimetric energy, missing only a small fraction of the total shower energy carried by muons and neutrinos.

The FD can only take data on clear, moonless nights, resulting in an up-time of around 14%. However, as it has been continuously operated since December 2004, it has a massive exposure [8]. Due to this, the FD is one of the few instruments which are directly sensitive to up-going air showers, and can be used to follow-up these ANITA observations. A general search for up-going showers has been performed using Monte-Carlo simulations for signal and background in a separate contribution [9]. Only events with elevation angles above 20 degrees have been considered because separation of upcoming and down going showers becomes less efficient as the showers become more horizontal. An integral upper limit of $3.6 \cdot 10^{-20} \text{cm}^{-2} \text{sr}^{-1} \text{s}^{-1}$, respectively $8.5 \cdot 10^{-20} \text{cm}^{-2} \text{sr}^{-1} \text{s}^{-1}$, for two different spectral indexes γ ($\gamma = -1$ and $\gamma = -2$) was obtained on the existence of up-going showers with a calorimetric energy $E_{\text{cal}} > 10^{17.5}$ eV [9].

Several possible interpretations involving physics Beyond Standard Model, *BSM*, have been proposed to interpret the ANITA anomalous events, such as sterile neutrino mixing [10], heavy dark matter [11], stau decays [12] or $L_e - L_\tau$ gauge interaction [13]. The search for up-going cosmic ray-like air showers at the Pierre Auger Observatory is recast in this work to a specific case as an

example. Here we consider the production of τ -lepton primaries by some unspecified mechanism. To widen the applicability of the results, in this work τ -leptons are generated in the Earth and atmosphere in proportion to media density without considering any specific model.

The generated τ -leptons are propagated taking into account energy loss inside the Earth until they decay using a modified version of NuTauSim [5] with the τ -decays being modeled with TAUOLA [14]. The resulting daughter particles are then evaluated in terms of their potential for producing an atmospheric air shower which can be measured by the FD. The resulting distribution of τ -decay induced air showers are binned in height of first interaction and shower energy. This 2-D distribution is then folded together with the double differential exposure of the Observatory to up-going events provided in [9] in three zenith angle ranges, shown again here for the full zenith range in Figure 1. As a result we obtain the effective exposure of the Observatory to up-going showers induced by τ -decay due to τ -leptons produced in the Earth by an unspecified mechanism, which is used to provide limits on the flux of these particles.

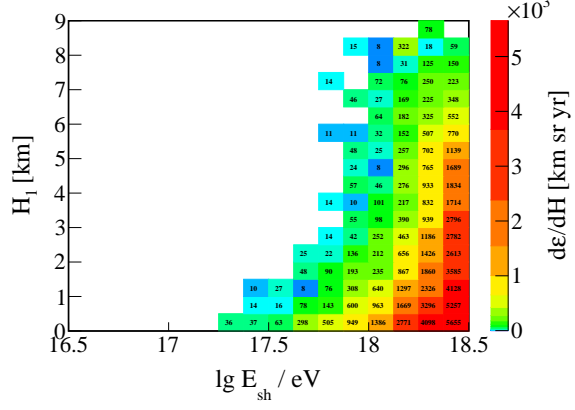


Figure 1: The double differential exposure of the FD to up-going showers from [9]

2. Simulation of τ -lepton primaries

For this study, simulated τ -leptons have been tracked from injection points both above and below the surface of the Earth with primary energies $E_0 \in [10^{16.5}, 10^{20}]$ eV, with $dN/dE \propto E^\gamma$ and $\gamma = -1, -2$. Due to energy loss and decay, the location of τ -lepton injection is of key importance. It is characterized by the distance from the injection point to the Earth's surface along the τ -lepton propagation axis, D_{inj} (negative when injected inside Earth and positive in the atmosphere). The τ -leptons are injected uniformly in a range of $D_{inj} \in [-50.0, 26.3]$ km. $D_{min} = -50$ km was chosen as lower limit because no τ -lepton injected further away exited the Earth with energies above $10^{16.5}$ eV in simulation. The maximum value of D_{inj} is chosen to match the exposure calculation in [9], namely $D_{max} = H_{max}/\cos \theta_{min} = 9.0/\cos 110^\circ \approx 26.3$ km, where H_{max} and the zenith angle θ_{min} are chosen according to the simulation parameters defined in [9].

The flat distribution of D_{inj} is then re-weighted using the media density at the injection point when it is above or below the surface of the Earth with:

$$w(H_{inj}) = \begin{cases} 1 & : H_{inj} \leq 0 \\ \frac{\rho_{atm}(H_{inj})}{\rho_{earth}} & : H_{inj} > 0 \end{cases}, \quad (1)$$

where $\rho_{atm}(H_{inj})$ is the average atmospheric density profile as a function of height above the Observatory, $H_{inj} = D_{inj} \cos \theta$ [15] and ρ_{earth} is taken as a constant 2.6 g cm^{-3} in the simulated depth range [5]. This is done so that the relative rate of τ -lepton production both in the Earth and

atmosphere correctly reflects relative interaction rates in matter as expected¹.

To track the propagation, energy-loss, and eventual decay of the generated τ -leptons, the simulation code developed for this study used NuTauSim [5] directly as a base. The main difference from the original version is that τ -leptons are directly generated rather than being produced from charged current interactions from injected τ -neutrinos. The τ -lepton propagation and tracking has been left entirely intact, however, the reporting of τ -decay products has been enhanced to directly report each daughter particle species along with its energy.

In the modified NuTauSim simulations, each generated τ is tracked until one of the six possible outcomes illustrated in Figure 2 occurs. In cases 1–4, the τ s are generated within the Earth and will be subject to energy losses through photo-nuclear processes, bremsstrahlung, and pair-production, until they either decay or escape to the atmosphere. In cases 5 and 6, the τ are generated directly in the atmosphere. Cases 1 and 2 are killed within the Earth either due to premature decay (1), or energy-loss to below the minimum threshold of $10^{16.5}$ eV (2). In cases 3–6, the τ must be tracked in the atmosphere where, because of the low density of the atmosphere, τ energy-loss is minimal and therefore neglected². As a result, τ can only either decay within the potential field-of-view of the FD, FD - FoV , (3 and 5), or escape the FD - FoV at which point they are killed (4 and 6). Only cases 3 and 5 contribute to the FD exposure to τ -leptons. All τ -leptons in cases 3 or 5 have the decay energy, E_{decay} . The distance from the surface of the Earth to the point of τ -decay, D_0 , is recorded for later simulation of the τ -decay and modeling of the resulting air shower.

Modeling τ -lepton decay induced showers The τ -decays for cases 3 and 5 above are simulated using TAUOLA [14], taking into account all decay branches. Of the particle species which can result from the τ -decay, only $\pi^\pm, \pi^0, K^\pm, K^0, e^\pm$ are considered to meaningfully contribute to the energy available to the resulting atmospheric air shower. Because of this, the energy of the resulting τ -decay induced shower is calculated as

$$E_{\text{sh}} = \sum_i E_i(E_{\text{decay}}), \quad (2)$$

where i iterates over $\pi^\pm, \pi^0, K^\pm, K^0, e^\pm$ and $E_i(E_{\text{decay}})$ is the energy of each daughter type calculated using E_{decay} . If the resulting $E_{\text{sh}} \in [10^{16.5}, 10^{18.5}]$ eV, then that event falls within the range of exposures reported in [9] and can therefore be used to adapt those results to a τ -primary case.

The FD exposure from [9], $\mathcal{E}(E_{\text{sh}}, H_1)$, shown in Figure 1, is given in terms of shower energy, E_{sh} and height of first interaction H_1 . Therefore, the point of first interaction of the resulting τ -induced air shower is also needed. The point of τ -decay, directly reported by the modified

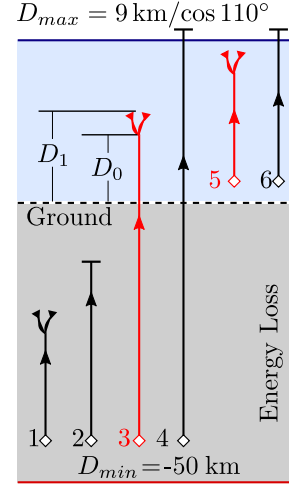


Figure 2: Representation of τ simulations. τ -decays which may trigger the FD are indicated in red

¹While production in the atmosphere is negligible in this case, this procedure allows for easy modification in case the production was due to other mechanisms such as exotic particle decays.

²This also has the consequence of removing all zenith dependence from the τ simulations as ρ_{earth} is a constant.

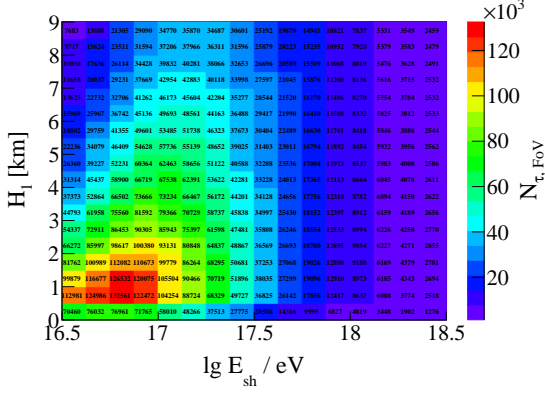


Figure 3: The distribution of τ -decay induced air showers within the FD-FoV.

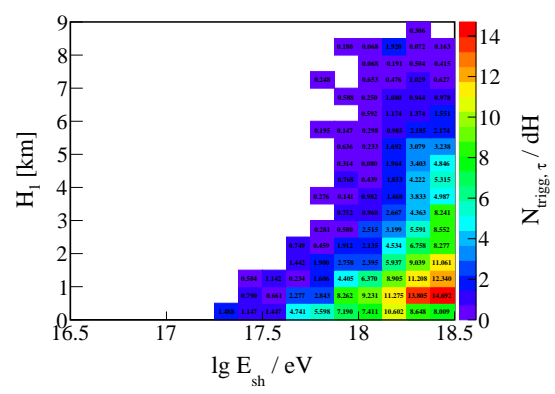


Figure 4: The distribution of τ -lepton induced air showers which would be selected as candidates in the FD analysis.

NuTauSim code for cases 3 and 5, must be extended by a depth X_1 , corresponding to the combined depth of first interaction of the daughter particles, on an event by event basis. X_1 is calculated by taking the average of the first interaction depths of the daughters particles, weighted by their energy:

$$X_1 = \sum_i X_1^i \cdot \frac{E_i}{E_{sh}}, \quad (3)$$

where i again iterates over $\pi^\pm, \pi^0, K^\pm, K^0, e^\pm$ and X_1^i is the mean depth of first interaction for each particle type (taken from CONEX [16]). To smooth the results, this procedure is carried out 100 times for each τ -decay and each result is given a weight of 1/100. The resulting distribution of X_1 is then folded together with the atmospheric density profile using the H_0 and θ of that event in order to calculate H_1 . Following this procedure for all generated τ -leptons in cases 3 and 5 results in the H_1 and E_{sh} distribution of τ -decay induced air showers shown in Figure 3. The distribution of selected τ -shower candidates which would trigger the FD and be selected in the up-going analysis is obtained by combining the two double differential histograms plotted in Figures 1 and 3 and is shown in Figure 4 for the entire zenith range. This procedure is also carried out separately for the three zenith sub-ranges provided in [9].

3. The exposure to τ -lepton decay induced showers

To calculate the exposure to τ -induced air showers as a function of the energy of the τ -lepton at the injection point, here-on called the primary energy, E_0 , all τ -induced showers produced in E_{sh} and H_1 space as described in the previous section, $N_{\tau, \text{FoV}}(E_{sh}, H_1)$, are back-tracked through the NuTauSim generation. Since each (E_{sh}, H_1) bin in $N_{\tau, \text{FoV}}(E_{sh}, H_1)$ is populated by τ -leptons events generated with many different E_0 values, each event in each $N_{\tau, \text{FoV}}(E_{sh}, H_1)$ bin must be back-tracked to its primary energy E_0 to obtain the distribution $N_{\tau, \text{FoV}}(E_0|E_{sh}, H_1)$. The triple differential exposure in E_0 , E_{sh} and H_1 is simply obtained multiplying the generic exposure, $\mathcal{E}(E_{sh}, H_1)$, numerically evaluated in [9], by the ratio of the induced number of showers and the primary number of generated events for primary tau-lepton energy E_0 :

$$\mathcal{E}_\tau(E_0|E_{sh}, H_1) = \frac{N_{\tau, \text{FoV}}(E_0|E_{sh}, H_1)}{N_{\text{gen}}(E_0)} \times \mathcal{E}(E_{sh}, H_1). \quad (4)$$

The final exposure is then obtained simply integrating $\mathcal{E}_\tau(E_0|E_{sh}, H_1)$ over the range of values of E_{sh} and H_1 considered, which is achieved by summing over all E_{sh} and H_1 bins:

$$\mathcal{E}_\tau(E_0) = \sum_{E_{sh}} \sum_{H_1} \mathcal{E}_\tau(E_0|E_{sh}, H_1). \quad (5)$$

This results in the FD exposure to τ generated with a less than 50 km path length below the surface of the Earth, which is plotted in Figure 5 (green symbols). This figure also displays the exposure for the three partial zenith angle sub-ranges considered in [9].

There are two behaviors visible in Figure 5 and therefore also in the limit plot shown below: a slow decrease in the rate growth of the exposure as energy increases and a quick flattening of the exposure just above $\sim 10^{18.7}$ eV. The slow decrease in the rate growth of the exposure as energy increases, is purely physical in origin. Here, the increase in FD sensitivity and τ -lepton survival rate in Earth as energy increases are competing with the quickly lengthening mean lifetime of the τ -leptons which causes an increasing number of τ to escape from the atmosphere without decaying. The quick flattening of the exposure, on the other hand, is understood as an edge effect related to the maximum shower energy of $10^{18.5}$ eV used in the general up-going search. As E_0 increases past this point, E_{sh} begins to also climb past this limit. Here, even though the FD sensitivity to these events would increase, the events are cut from the analysis because we still lack exposure information at these energies. However, this decrease is partially compensated for by the increasing rate at which τ survive to the surface, leaving the exposure almost flat above these energies.

If the energy range of the general study were to be increased past $10^{18.5}$ eV to higher energies, the exposure would continue to increase past $\sim 10^{18.7}$ eV while the rate of exposure increase would continue to slow down. At some energy, the increases in FD sensitivity and τ survival would be insufficient to compensate for the longer τ -lifetime and the exposure would peak, flatten and then decrease. This increase in the maximum shower energies in the general analysis would of course also translate to even lower upper limits than those provided below. This improvement to the study is planned for the near future.

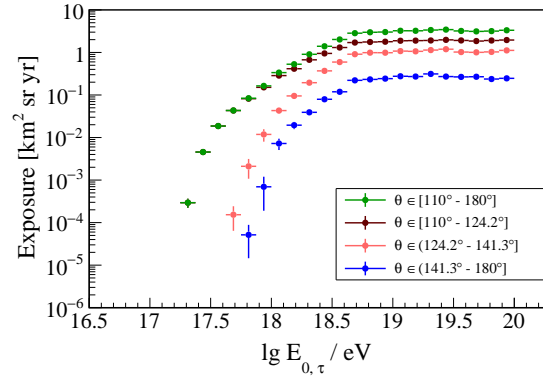


Figure 5: Exposure to up-going τ -induced air showers as a function of primary energy and zenith angle.

4. Flux limits

From the background simulations carried out in the general search [9], a background expectation N_{bkg} of 0.5 events was found for the full evaluated energy range. After the data unbinding we get 1 event passing the analysis cuts, which is consistent with the background expectations. Using the Feldman Cousins approach, the limit that can be obtained at 95% C.L. when 1 event is observed and 0.5 events are expected as background, corresponds to the flux that would give an expected number of events $N_{FC} = 4.05$. To calculate the differential flux limits in terms of τ -lepton primary energy, the events are back tracked to the specific primary energy distribution as explained above.

Then, the number of FC candidates required per E_0 bin, $N_{\text{FC}}(E_0)$, can be calculated as

$$N_{\text{FC}}(E_0) = \frac{N_{\text{FC}}/N_{\text{bins}}}{\mathcal{E}_\tau(E_0) \cdot w_\gamma(E_0) / \sum_{E_0 \text{ bins}} (\mathcal{E}_\tau(E_0) \cdot w_\gamma(E_0))} \quad (6)$$

where $w_\gamma(E_0) \propto E_0^{\gamma+1}$ inherently depends on the energy spectral index, γ , which the τ primaries are injected with. The effects of the spectrum are therefore folded into $N_{\text{FC}}(E_0)$. Finally, the flux limits can be calculated by using the exposure defined in Eq. 5 to translate $N_{\text{FC}}(E_0)$ into flux as:

$$\Phi_\tau^{95\%}(E_0) = \frac{N_{\text{FC}}(E_0)}{\mathcal{E}_\tau(E_0)}. \quad (7)$$

Following the procedure described above, upper limits against the primary energy for different τ -lepton energy spectra are presented for the entire zenith angle range in Figure 6. Since the simulated τ -leptons are uniformly produced below the surface, the limits are provided both in terms of flux of τ -leptons created within 50 km of path length below the Earth's surface (left scale on the y-axis), as well as in terms of the rate of τ -leptons generated per unit volume, energy and solid angle (right scale on the y-axis) which may be more convenient to compare to specific models producing τ -leptons uniformly below the Earth's surface. For a spectral index of $\gamma = -1$ the flux limits follow the trends present in the exposure plot. The limits for an energy spectrum of $\gamma = -2$ also follow the trend in Figure 6, however here the limits worsen after $10^{18.7}$ eV. The upper flux limits for the three zenith angle sub-ranges have also been calculated and are plotted in Figure 7. As expected from the exposure, the most horizontal zenith angles provide the best limits.

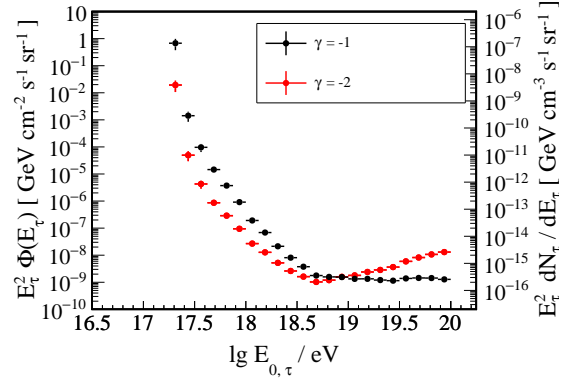


Figure 6: Flux Upper limits for τ -induced air showers with $CI = 95\%$ for different primary energy spectra

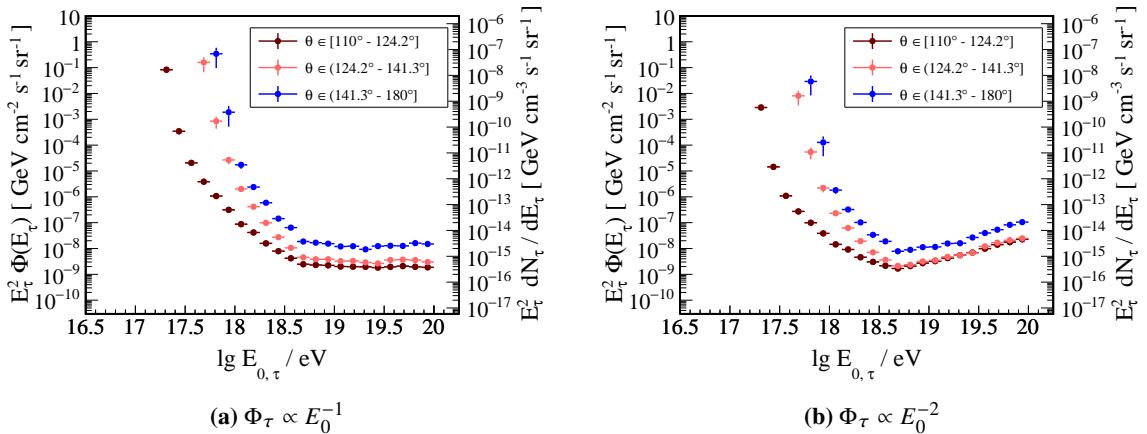


Figure 7: $CI = 95\%$ upper-limit to τ -lepton flux at 50 km under the Earth surface vs E_0 energy for 1 event passing the analysis cuts, consistent with $N_{\text{bkg}} = 0.5$, for different τ energy spectra and zenith angle ranges.

5. Conclusions

The response of the fluorescence detector of the Pierre Auger Observatory to up-going τ -induced air showers has been studied. This was accomplished by simulating τ -leptons in a zenith range of 110° – 180° generated both below and above Earth. For a maximal flexibility, the τ -leptons are generated in a way that ignores their production mechanism. The τ -leptons are propagated through the Earth and followed through the atmosphere until they reach the maximum height of 9 km defined in [9]. All recorded τ -decays in the FD-FoV are then used to estimate the exposure of the FD to up-going showers induced by τ -decay, using the double differential exposure distribution provided in the general study. This is then translated to flux limits to up-going τ within a maximum range of 50 km below the Earth's crust to 9 km above it.

Both the exposure results and the upper flux limits have been calculated for the whole zenith range of interest, as well as for three different zenith sub-ranges. The highest exposure is obtained for the most horizontal zenith angles. Flux upper limits for a $CI = 95\%$ have been calculated for different primary energy spectra. As in the exposure case, the best flux limits are obtained for the most horizontal zenith angles. Since the general study case represents the skeleton of the analysis, the presented results are strongly influenced by the maximum energy considered within the simulations. This can be clearly seen in the exposure plots, which are peaked at the corresponding τ -lepton primary energy. The current flux limits and exposure results are therefore corresponding to τ induced air showers in a sensitive volume of the FD of the Pierre Auger Observatory limited to a maximum shower energy of $10^{18.5}$ eV.

By using the presented results with the given values for the upper flux limits and exposure one can test different BSM scenarios which produce τ -leptons. By folding in the respective cross sections, upper flux limits can be calculated against various theoretical models.

References

- [1] P.W. Gorham et al., [ANITA Coll.], *Phys. Rev. Lett.* **121** (2018) 161102.
- [2] A. Romero-Wolf et al., *Phys. Rev. D* **99** (2019) 063011 [1811.07261].
- [3] M.G. Aartsen et al., [IceCube Coll.], 2001.01737.
- [4] A. Aab et al., [Pierre Auger Coll.], *Phys. Rev. D* **91** (2015) 092008 [1504.05397].
- [5] J. Alvarez-Muñiz et al., *Phys. Rev. D* **97** (2018) 023021 [Erratum: Phys.Rev.D 99, 069902 (2019)].
- [6] D.B. Fox, S. Sigurdsson, S. Shandera, P. Mészáros, K. Murase, M. Mostafá et al., 1809.09615.
- [7] S. Chipman, R. Diesing, M.H. Reno and I. Sarcevic, *Phys. Rev. D* **100** (2019) 063011.
- [8] P. Abreu et al., [Pierre Auger Coll.], *Astropart. Phys.* **34** (2011) 368.
- [9] M. Mastrodicasa for the [Pierre Auger Coll.], these proceedings.
- [10] G.-y. Huang, *Phys. Rev. D* **98** (2018) 043019 [1804.05362].
- [11] L. Heurtier, D. Kim, J.-C. Park and S. Shin, *Phys. Rev. D* **100** (2019) 055004 [1905.13223].
- [12] A. Connolly, P. Allison and O. Banerjee, *arXiv e-prints* (2018) [1807.08892].
- [13] A. Esmaili and Y. Farzan, *JCAP* **12** (2019) 017 [1909.07995].
- [14] M. Chrzaszcz, T. Przedzinski, Z. Was and J. Zaremba, *Comput. Phys. Commun.* **232** (2018) 220.
- [15] U.S.C. on Extension to the Standard Atmosphere., U.S. standard atmosphere (1976).
- [16] T. Pierog et al., *Nucl. Phys. B Proc. Suppl.* **151** (2006) 159 [astro-ph/0411260].

The Pierre Auger Collaboration



PIERRE
AUGER
OBSERVATORY

P. Abreu⁷², M. Aglietta^{54,52}, J.M. Albury¹³, I. Allekotte¹, A. Almela^{8,12}, J. Alvarez-Muñiz⁷⁹, R. Alves Batista⁸⁰, G.A. Anastasi^{63,52}, L. Anchordoqui⁸⁷, B. Andrada⁸, S. Andringa⁷², C. Aramo⁵⁰, P.R. Araújo Ferreira⁴², J. C. Arteaga Velázquez⁶⁷, H. Asorey⁸, P. Assis⁷², G. Avila¹¹, A.M. Badescu⁷⁵, A. Bakalova³², A. Balaceanu⁷³, F. Barbato^{45,46}, R.J. Barreira Luz⁷², K.H. Becker³⁸, J.A. Bellido^{13,69}, C. Berat³⁶, M.E. Bertaina^{63,52}, X. Bertou¹, P.L. Biermann^b, V. Binet⁶, K. Bismark^{39,8}, T. Bister⁴², J. Biteau³⁷, J. Blazek³², C. Bleve³⁶, M. Boháčová³², D. Boncioli^{57,46}, C. Bonifazi^{9,26}, L. Bonneau Arbeletche²¹, N. Borodai⁷⁰, A.M. Botti⁸, J. Brack^d, T. Bretz⁴², P.G. Brichetto Orcherá⁸, F.L. Brichele⁴², P. Buchholz⁴⁴, A. Bueno⁷⁸, S. Buitink¹⁵, M. Buscemi⁴⁷, M. Büsken^{39,8}, K.S. Caballero-Mora⁶⁶, L. Caccianiga^{59,49}, F. Canfora^{80,81}, I. Caracas³⁸, J.M. Carceller⁷⁸, R. Caruso^{58,47}, A. Castellina^{54,52}, F. Catalani¹⁹, G. Cataldi⁴⁸, L. Cazon⁷², M. Cerda¹⁰, J.A. Chinellato²², J. Chudoba³², L. Chytka³³, R.W. Clay¹³, A.C. Cobos Cerutti⁷, R. Colalillo^{60,50}, A. Coleman⁹³, M.R. Coluccia⁴⁸, R. Conceição⁷², A. Condorelli^{45,46}, G. Consolati^{49,55}, F. Contreras¹¹, F. Convenga^{56,48}, D. Correia dos Santos²⁸, C.E. Covault⁸⁵, S. Dasso^{5,3}, K. Daumiller⁴¹, B.R. Dawson¹³, J.A. Day¹³, R.M. de Almeida²⁸, J. de Jesús^{8,41}, S.J. de Jong^{80,81}, G. De Mauro^{80,81}, J.R.T. de Mello Neto^{26,27}, I. De Mitri^{45,46}, J. de Oliveira¹⁸, D. de Oliveira Franco²², F. de Palma^{56,48}, V. de Souza²⁰, E. De Vito^{56,48}, M. del Río¹¹, O. Deligny³⁴, L. Deval^{41,8}, A. di Matteo⁵², C. Dobrigkeit²², J.C. D'Olivo⁶⁸, L.M. Domingues Mendes⁷², R.C. dos Anjos²⁵, D. dos Santos²⁸, M.T. Dova⁴, J. Ebr³², R. Engel^{39,41}, I. Epicoco^{56,48}, M. Erdmann⁴², C.O. Escobar^a, A. Etchegoyen^{8,12}, H. Falcke^{80,82,81}, J. Farmer⁹², G. Farrar⁹⁰, A.C. Fauth²², N. Fazzini^a, F. Feldbusch⁴⁰, F. Fenu^{54,52}, B. Fick⁸⁹, J.M. Figueira⁸, A. Filipčić^{77,76}, T. Fitoussi⁴¹, T. Fodran⁸⁰, M.M. Freire⁶, T. Fujii^{92,e}, A. Fuster^{8,12}, C. Galea⁸⁰, C. Galelli^{59,49}, B. García⁷, A.L. Garcia Vegas⁴², H. Gemmeke⁴⁰, F. Gesualdi^{8,41}, A. Gherghel-Lascu⁷³, P.L. Ghia³⁴, U. Giaccari⁸⁰, M. Giammarchi⁴⁹, J. Glombitza⁴², F. Gobbi¹⁰, F. Gollan⁸, G. Golup¹, M. Gómez Berisso¹, P.F. Gómez Vitale¹¹, J.P. Gongora¹¹, J.M. González¹, N. González¹⁴, I. Goos^{1,41}, D. Góra⁷⁰, A. Gorgi^{54,52}, M. Gottowik³⁸, T.D. Grubb¹³, F. Guarino^{60,50}, G.P. Guedes²³, E. Guido^{52,63}, S. Hahn^{41,8}, P. Hamal³², M.R. Hampel⁸, P. Hansen⁴, D. Harari¹, V.M. Harvey¹³, A. Haungs⁴¹, T. Hebbeker⁴², D. Heck⁴¹, G.C. Hill¹³, C. Hojvat^a, J.R. Hörandel^{80,81}, P. Horvath³³, M. Hrabovský³³, T. Huege^{41,15}, A. Insolia^{58,47}, P.G. Isar⁷⁴, P. Janecek³², J.A. Johnsen⁸⁶, J. Jurysek³², A. Kääpä³⁸, K.H. Kampert³⁸, N. Karastathis⁴¹, B. Keilhauer⁴¹, J. Kemp⁴², A. Khakurdikar⁸⁰, V.V. Kizakke Covilakam^{8,41}, H.O. Klages⁴¹, M. Kleifges⁴⁰, J. Kleinfeller¹⁰, M. Köpke³⁹, N. Kunka⁴⁰, B.L. Lago¹⁷, R.G. Lang²⁰, N. Langner⁴², M.A. Leigui de Oliveira²⁴, V. Lenok⁴¹, A. Letessier-Selvon³⁵, I. Lhenry-Yvon³⁴, D. Lo Presti^{58,47}, L. Lopes⁷², R. López⁶⁴, L. Lu⁹⁴, Q. Luce³⁹, J.P. Lundquist⁷⁶, A. Machado Payeras²², G. Mancarella^{56,48}, D. Mandat³², B.C. Manning¹³, J. Manshanden⁴³, P. Mantsch^a, S. Marafico³⁴, A.G. Mariuzzi⁴, I.C. Mariş¹⁴, G. Marsella^{61,47}, D. Martello^{56,48}, S. Martinelli^{41,8}, O. Martínez Bravo⁶⁴, M. Mastrodicasa^{57,46}, H.J. Mathes⁴¹, J. Matthews⁸⁸, G. Matthiae^{62,51}, E. Mayotte³⁸, P.O. Mazur^a, G. Medina-Tanco⁶⁸, D. Melo⁸, A. Menshikov⁴⁰, K.-D. Merenda⁸⁶, S. Michal³³, M.I. Micheletti⁶, L. Miramonti^{59,49}, S. Mollerach¹, F. Montanet³⁶, C. Morello^{54,52}, M. Mostafá⁹¹, A.L. Müller⁸, M.A. Muller²², K. Mulrey¹⁵, R. Mussa⁵², M. Muzio⁹⁰, W.M. Namasaka³⁸, A. Nasr-Esfahani³⁸, L. Nellen⁶⁸, M. Niculescu-Oglinazu⁷³, M. Niechciol⁴⁴, D. Nitz⁸⁹, D. Nosek³¹, V. Novotny³¹, L. Nožka³³, A. Nucita^{56,48}, L.A. Núñez³⁰, M. Palatka³², J. Pallotta², P. Papenbreer³⁸, G. Parente⁷⁹, A. Parra⁶⁴, J. Pawlowsky³⁸, M. Pech³², F. Pedreira⁷⁹, J. Peřkala⁷⁰, R. Pelayo⁶⁵, J. Peña-Rodríguez³⁰, E.E. Pereira Martins^{39,8}, J. Perez Armand²¹, C. Pérez Bertoli^{8,41}, M. Perlin^{8,41}, L. Perrone^{56,48}, S. Petrera^{45,46}, T. Pierog⁴¹, M. Pimenta⁷², V. Pirronello^{58,47}, M. Platino⁸, B. Pont⁸⁰, M. Pothast^{81,80}, P. Privitera⁹², M. Prouza³², A. Puyleart⁸⁹, S. Querchfeld³⁸, J. Rautenberg³⁸, D. Ravnani⁸, M. Reininghaus^{41,8}, J. Ridky³², F. Riehn⁷², M. Risse⁴⁴, V. Rizi^{57,46}, W. Rodrigues de Carvalho²¹, J. Rodríguez Rojo¹¹, M.J. Roncoroni⁸, S. Rossoni⁴³, M. Roth⁴¹, E. Roulet¹, A.C. Rovero⁵, P. Ruehl⁴⁴, A. Saftoiu⁷³,

F. Salamida^{57,46}, H. Salazar⁶⁴, G. Salina⁵¹, J.D. Sanabria Gomez³⁰, F. Sánchez⁸, E.M. Santos²¹, E. Santos³², F. Sarazin⁸⁶, R. Sarmiento⁷², C. Sarmiento-Cano⁸, R. Sato¹¹, P. Savina^{56,48,34,94}, C.M. Schäfer⁴¹, V. Scherini^{56,48}, H. Schieler⁴¹, M. Schimassek^{39,8}, M. Schimp³⁸, F. Schlüter^{41,8}, D. Schmidt³⁹, O. Scholten^{84,15}, P. Schovánek³², F.G. Schröder^{93,41}, S. Schröder³⁸, J. Schulte⁴², S.J. Sciutto⁴, M. Scornavacche^{8,41}, A. Segreto^{53,47}, S. Sehgal³⁸, R.C. Shellard¹⁶, G. Sigl⁴³, G. Silli^{8,41}, O. Sima^{73,f}, R. Šmída⁹², P. Sommers⁹¹, J.F. Soriano⁸⁷, J. Souchard³⁶, R. Squartini¹⁰, M. Stadelmaier^{41,8}, D. Stanca⁷³, S. Stanič⁷⁶, J. Stasielak⁷⁰, P. Stassi³⁶, A. Streich^{39,8}, M. Suárez-Durán¹⁴, T. Sudholz¹³, T. Suomijärvi³⁷, A.D. Supanitsky⁸, Z. Szadkowski⁷¹, A. Tapia²⁹, C. Taricco^{63,52}, C. Timmermans^{81,80}, O. Tkachenko⁴¹, P. Tobiska³², C.J. Todero Peixoto¹⁹, B. Tome⁷², Z. Torrès³⁶, A. Travaini¹⁰, P. Travnicek³², C. Trimarelli^{57,46}, M. Tueros⁴, R. Ulrich⁴¹, M. Unger⁴¹, L. Vaclavek³³, M. Vacula³³, J.F. Valdés Galicia⁶⁸, L. Valore^{60,50}, E. Varela⁶⁴, A. Vásquez-Ramírez³⁰, D. Veberič⁴¹, C. Ventura²⁷, I.D. Vergara Quispe⁴, V. Verzi⁵¹, J. Vicha³², J. Vink⁸³, S. Vorobiov⁷⁶, H. Wahlberg⁴, C. Watanabe²⁶, A.A. Watson^c, M. Weber⁴⁰, A. Weindl⁴¹, L. Wiencke⁸⁶, H. Wilczyński⁷⁰, M. Wirtz⁴², D. Wittkowski³⁸, B. Wundheiler⁸, A. Yushkov³², O. Zapparrata¹⁴, E. Zas⁷⁹, D. Zavrtanik^{76,77}, M. Zavrtanik^{77,76}, L. Zehrer⁷⁶

— • —

- ¹ Centro Atómico Bariloche and Instituto Balseiro (CNEA-UNCuyo-CONICET), San Carlos de Bariloche, Argentina
- ² Centro de Investigaciones en Láseres y Aplicaciones, CITEDEF and CONICET, Villa Martelli, Argentina
- ³ Departamento de Física and Departamento de Ciencias de la Atmósfera y los Océanos, FCEyN, Universidad de Buenos Aires and CONICET, Buenos Aires, Argentina
- ⁴ IFLP, Universidad Nacional de La Plata and CONICET, La Plata, Argentina
- ⁵ Instituto de Astronomía y Física del Espacio (IAFE, CONICET-UBA), Buenos Aires, Argentina
- ⁶ Instituto de Física de Rosario (IFIR) – CONICET/U.N.R. and Facultad de Ciencias Bioquímicas y Farmacéuticas U.N.R., Rosario, Argentina
- ⁷ Instituto de Tecnologías en Detección y Astropartículas (CNEA, CONICET, UNSAM), and Universidad Tecnológica Nacional – Facultad Regional Mendoza (CONICET/CNEA), Mendoza, Argentina
- ⁸ Instituto de Tecnologías en Detección y Astropartículas (CNEA, CONICET, UNSAM), Buenos Aires, Argentina
- ⁹ International Center of Advanced Studies and Instituto de Ciencias Físicas, ECyT-UNSAM and CONICET, Campus Miguelete – San Martín, Buenos Aires, Argentina
- ¹⁰ Observatorio Pierre Auger, Malargüe, Argentina
- ¹¹ Observatorio Pierre Auger and Comisión Nacional de Energía Atómica, Malargüe, Argentina
- ¹² Universidad Tecnológica Nacional – Facultad Regional Buenos Aires, Buenos Aires, Argentina
- ¹³ University of Adelaide, Adelaide, S.A., Australia
- ¹⁴ Université Libre de Bruxelles (ULB), Brussels, Belgium
- ¹⁵ Vrije Universiteit Brussels, Brussels, Belgium
- ¹⁶ Centro Brasileiro de Pesquisas Físicas, Rio de Janeiro, RJ, Brazil
- ¹⁷ Centro Federal de Educação Tecnológica Celso Suckow da Fonseca, Nova Friburgo, Brazil
- ¹⁸ Instituto Federal de Educação, Ciência e Tecnologia do Rio de Janeiro (IFRJ), Brazil
- ¹⁹ Universidade de São Paulo, Escola de Engenharia de Lorena, Lorena, SP, Brazil
- ²⁰ Universidade de São Paulo, Instituto de Física de São Carlos, São Carlos, SP, Brazil
- ²¹ Universidade de São Paulo, Instituto de Física, São Paulo, SP, Brazil
- ²² Universidade Estadual de Campinas, IFGW, Campinas, SP, Brazil
- ²³ Universidade Estadual de Feira de Santana, Feira de Santana, Brazil
- ²⁴ Universidade Federal do ABC, Santo André, SP, Brazil
- ²⁵ Universidade Federal do Paraná, Setor Palotina, Palotina, Brazil
- ²⁶ Universidade Federal do Rio de Janeiro, Instituto de Física, Rio de Janeiro, RJ, Brazil
- ²⁷ Universidade Federal do Rio de Janeiro (UFRJ), Observatório do Valongo, Rio de Janeiro, RJ, Brazil
- ²⁸ Universidade Federal Fluminense, EEIMVR, Volta Redonda, RJ, Brazil
- ²⁹ Universidad de Medellín, Medellín, Colombia
- ³⁰ Universidad Industrial de Santander, Bucaramanga, Colombia

- ³¹ Charles University, Faculty of Mathematics and Physics, Institute of Particle and Nuclear Physics, Prague, Czech Republic
- ³² Institute of Physics of the Czech Academy of Sciences, Prague, Czech Republic
- ³³ Palacky University, RCPTM, Olomouc, Czech Republic
- ³⁴ CNRS/IN2P3, IJCLab, Université Paris-Saclay, Orsay, France
- ³⁵ Laboratoire de Physique Nucléaire et de Hautes Energies (LPNHE), Sorbonne Université, Université de Paris, CNRS-IN2P3, Paris, France
- ³⁶ Univ. Grenoble Alpes, CNRS, Grenoble Institute of Engineering Univ. Grenoble Alpes, LPSC-IN2P3, 38000 Grenoble, France
- ³⁷ Université Paris-Saclay, CNRS/IN2P3, IJCLab, Orsay, France
- ³⁸ Bergische Universität Wuppertal, Department of Physics, Wuppertal, Germany
- ³⁹ Karlsruhe Institute of Technology (KIT), Institute for Experimental Particle Physics, Karlsruhe, Germany
- ⁴⁰ Karlsruhe Institute of Technology (KIT), Institut für Prozessdatenverarbeitung und Elektronik, Karlsruhe, Germany
- ⁴¹ Karlsruhe Institute of Technology (KIT), Institute for Astroparticle Physics, Karlsruhe, Germany
- ⁴² RWTH Aachen University, III. Physikalisches Institut A, Aachen, Germany
- ⁴³ Universität Hamburg, II. Institut für Theoretische Physik, Hamburg, Germany
- ⁴⁴ Universität Siegen, Department Physik – Experimentelle Teilchenphysik, Siegen, Germany
- ⁴⁵ Gran Sasso Science Institute, L'Aquila, Italy
- ⁴⁶ INFN Laboratori Nazionali del Gran Sasso, Assergi (L'Aquila), Italy
- ⁴⁷ INFN, Sezione di Catania, Catania, Italy
- ⁴⁸ INFN, Sezione di Lecce, Lecce, Italy
- ⁴⁹ INFN, Sezione di Milano, Milano, Italy
- ⁵⁰ INFN, Sezione di Napoli, Napoli, Italy
- ⁵¹ INFN, Sezione di Roma “Tor Vergata”, Roma, Italy
- ⁵² INFN, Sezione di Torino, Torino, Italy
- ⁵³ Istituto di Astrofisica Spaziale e Fisica Cosmica di Palermo (INAF), Palermo, Italy
- ⁵⁴ Osservatorio Astrofisico di Torino (INAF), Torino, Italy
- ⁵⁵ Politecnico di Milano, Dipartimento di Scienze e Tecnologie Aerospaziali, Milano, Italy
- ⁵⁶ Università del Salento, Dipartimento di Matematica e Fisica “E. De Giorgi”, Lecce, Italy
- ⁵⁷ Università dell’Aquila, Dipartimento di Scienze Fisiche e Chimiche, L’Aquila, Italy
- ⁵⁸ Università di Catania, Dipartimento di Fisica e Astronomia, Catania, Italy
- ⁵⁹ Università di Milano, Dipartimento di Fisica, Milano, Italy
- ⁶⁰ Università di Napoli “Federico II”, Dipartimento di Fisica “Ettore Pancini”, Napoli, Italy
- ⁶¹ Università di Palermo, Dipartimento di Fisica e Chimica “E. Segrè”, Palermo, Italy
- ⁶² Università di Roma “Tor Vergata”, Dipartimento di Fisica, Roma, Italy
- ⁶³ Università Torino, Dipartimento di Fisica, Torino, Italy
- ⁶⁴ Benemérita Universidad Autónoma de Puebla, Puebla, México
- ⁶⁵ Unidad Profesional Interdisciplinaria en Ingeniería y Tecnologías Avanzadas del Instituto Politécnico Nacional (UPIITA-IPN), México, D.F., México
- ⁶⁶ Universidad Autónoma de Chiapas, Tuxtla Gutiérrez, Chiapas, México
- ⁶⁷ Universidad Michoacana de San Nicolás de Hidalgo, Morelia, Michoacán, México
- ⁶⁸ Universidad Nacional Autónoma de México, México, D.F., México
- ⁶⁹ Universidad Nacional de San Agustín de Arequipa, Facultad de Ciencias Naturales y Formales, Arequipa, Peru
- ⁷⁰ Institute of Nuclear Physics PAN, Krakow, Poland
- ⁷¹ University of Łódź, Faculty of High-Energy Astrophysics, Łódź, Poland
- ⁷² Laboratório de Instrumentação e Física Experimental de Partículas – LIP and Instituto Superior Técnico – IST, Universidade de Lisboa – UL, Lisboa, Portugal
- ⁷³ “Horia Hulubei” National Institute for Physics and Nuclear Engineering, Bucharest-Magurele, Romania
- ⁷⁴ Institute of Space Science, Bucharest-Magurele, Romania
- ⁷⁵ University Politehnica of Bucharest, Bucharest, Romania
- ⁷⁶ Center for Astrophysics and Cosmology (CAC), University of Nova Gorica, Nova Gorica, Slovenia
- ⁷⁷ Experimental Particle Physics Department, J. Stefan Institute, Ljubljana, Slovenia

- ⁷⁸ Universidad de Granada and C.A.F.P.E., Granada, Spain
- ⁷⁹ Instituto Galego de Física de Altas Enerxías (IGFAE), Universidade de Santiago de Compostela, Santiago de Compostela, Spain
- ⁸⁰ IMAPP, Radboud University Nijmegen, Nijmegen, The Netherlands
- ⁸¹ Nationaal Instituut voor Kernfysica en Hoge Energie Fysica (NIKHEF), Science Park, Amsterdam, The Netherlands
- ⁸² Stichting Astronomisch Onderzoek in Nederland (ASTRON), Dwingeloo, The Netherlands
- ⁸³ Universiteit van Amsterdam, Faculty of Science, Amsterdam, The Netherlands
- ⁸⁴ University of Groningen, Kapteyn Astronomical Institute, Groningen, The Netherlands
- ⁸⁵ Case Western Reserve University, Cleveland, OH, USA
- ⁸⁶ Colorado School of Mines, Golden, CO, USA
- ⁸⁷ Department of Physics and Astronomy, Lehman College, City University of New York, Bronx, NY, USA
- ⁸⁸ Louisiana State University, Baton Rouge, LA, USA
- ⁸⁹ Michigan Technological University, Houghton, MI, USA
- ⁹⁰ New York University, New York, NY, USA
- ⁹¹ Pennsylvania State University, University Park, PA, USA
- ⁹² University of Chicago, Enrico Fermi Institute, Chicago, IL, USA
- ⁹³ University of Delaware, Department of Physics and Astronomy, Bartol Research Institute, Newark, DE, USA
- ⁹⁴ University of Wisconsin-Madison, Department of Physics and WIPAC, Madison, WI, USA
-
- ^a Fermi National Accelerator Laboratory, Fermilab, Batavia, IL, USA
- ^b Max-Planck-Institut für Radioastronomie, Bonn, Germany
- ^c School of Physics and Astronomy, University of Leeds, Leeds, United Kingdom
- ^d Colorado State University, Fort Collins, CO, USA
- ^e now at Hakubi Center for Advanced Research and Graduate School of Science, Kyoto University, Kyoto, Japan
- ^f also at University of Bucharest, Physics Department, Bucharest, Romania